Supporting Information

The influence of the Li^+ addition rate during the hydrothermal synthesis of $LiFePO_4$ on the average and local structure

Michelle Thiebaut,[a,b] Caren Billing,[a,b*] Deena Naidoo[c] and David G. Billing[a,b]

[1]Molecular Science Institute, School of Chemistry, University of the Witwatersrand, Private Bag X3, Johannesburg 2050, South Africa

[2]DST-NRF Centre of Excellence in Strong Materials, University of the Witwatersrand, Private Bag X3, 2050 Johannesburg, South Africa

[3]Material Physics Research Institute, School of Physics, University of the Witwatersrand, Private Bag X3, Johannesburg 2050, South Africa

*Email: caren.billing@wits.ac.za; Tel.: +27 11 717 6768

1. Homemade Teflon bombs

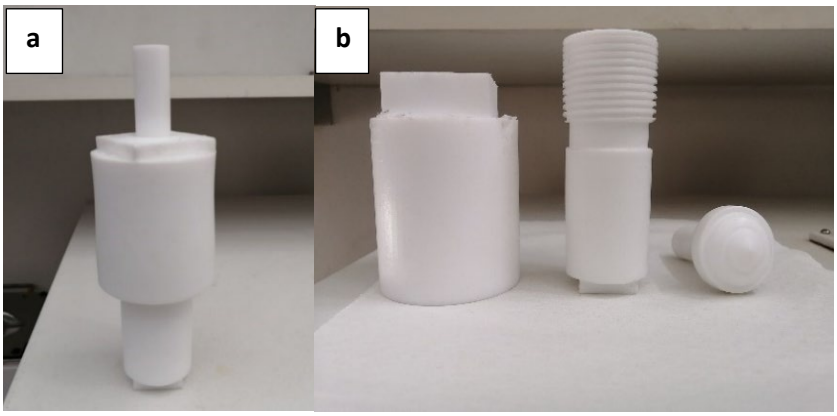

Fig S1: An example of the Teflon reaction vessels used for the hydrothermal synthesis which shows (a) the fully assembled and (b) the deconstructed components.

2. Rietveld refinement calibration plot

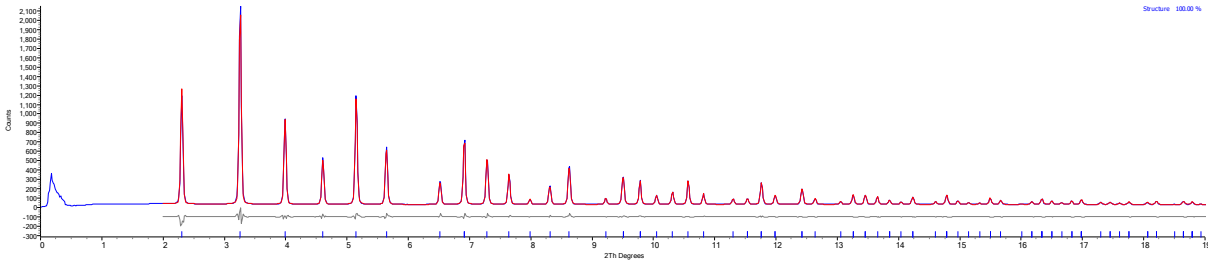

Fig. S2 Rietveld refinement plot of the calibration plot of the 28-ID-1 BNL LaB_6 (NIST 660c) sample.

Table S1 Structural parameters extracted from the 28-ID-1 BNL LaB_6 (NIST 660c) refinement.

Structural parameter	Refined value
Wavelength /Å	0.167057(4)
R-factors	R_{wp} = 4.06 R_p = 2.99 R_{exp} = 12.99
GOF	0.31

3. Rietveld refinement plots of the varied Li^+ addition rate samples

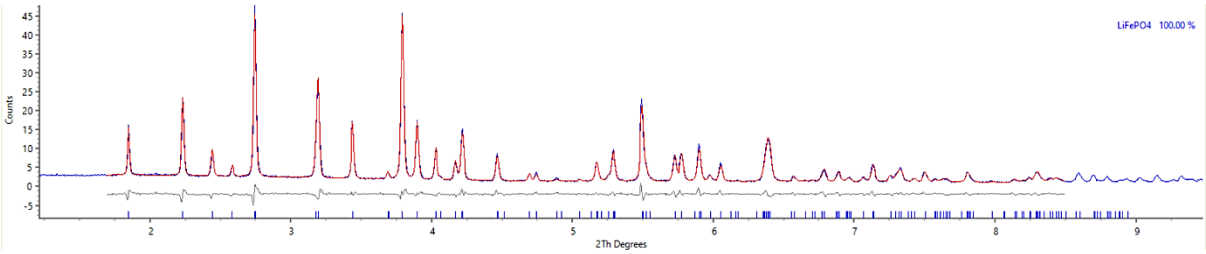

Fig. S3 Rietveld refinement plot of the 1sec Li^+ addition rate sample.

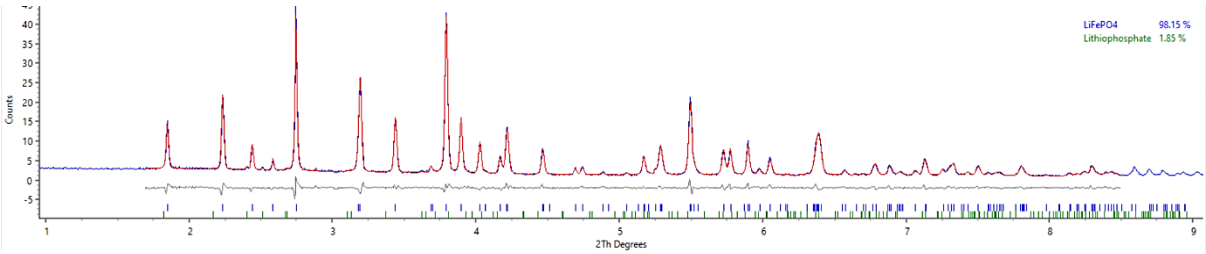

Fig. S4 Rietveld refinement plot of the 3sec Li^+ addition rate sample.

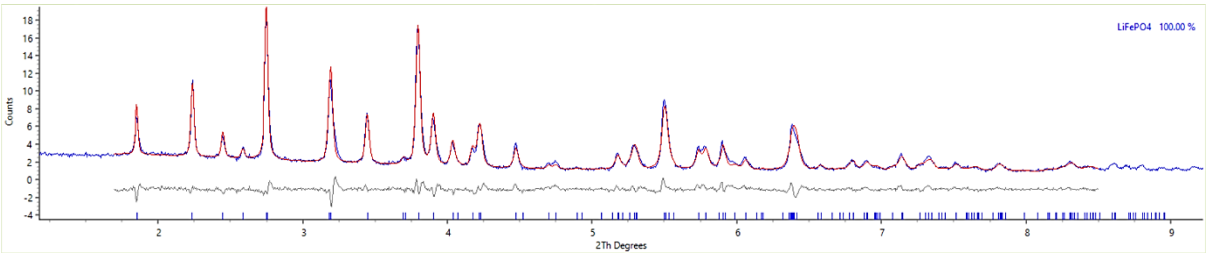

Fig. S5 Rietveld refinement plot of the 4sec Li^+ addition rate sample.

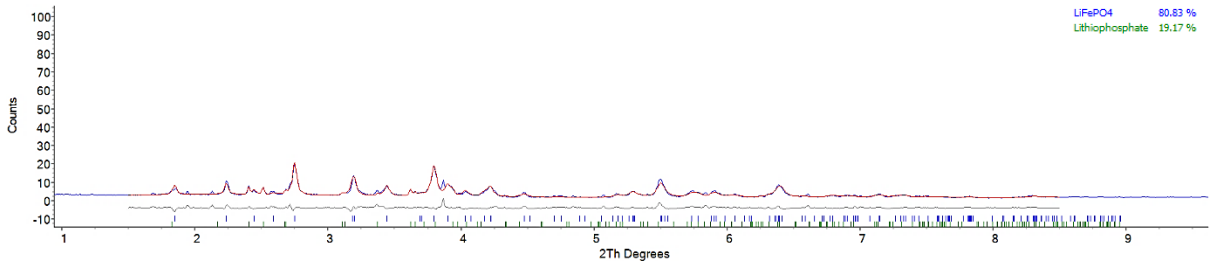

Fig. S6 Rietveld refinement plot of the 5sec Li^+ addition rate sample.

Data from the Rietveld refinements are presented as the crystal and structural parameters in Table S2 and the fractional coordinates, site occupancy factors (S.O.F.) and the displacement parameters (B_{iso}) of the $LiFePO_4$ phase in Tables S3-S6 for each sample. During each of the refinements the isotropic displacement parameters (thermal parameters, B_{iso}) and site occupancy factors (S.O.F.'s) for Fe and Li were simultaneously refined as independent parameters and all refined to reasonable values. Additionally, the powder CIF files generated for each refinement are included as

supplementary information. These can readily be used to visualise the Rietveld refinement details using the program pdCIFplotter from Matthew Rowles (https://doi.org/10.1107/S1600576722003478) and for further details about each refinement.

Table S2 The crystal and structural parameters as determined with the refinement of the Li^+ addition rate samples.

	1sec	3sec		4sec	5sec#	
Phase	$LiFePO_4$ (100 %)	$LiFePO_4$ (98.15%)	Li_3PO_4 (1.85 %)	$LiFePO_4$ (100 %)	$LiFePO_4$ (80.83%)	Li_3PO_4 (19.17 %)
Crystal system	Orthorhombic	Orthorhombic	Orthorhombic	Orthorhombic	Orthorhombic	Orthorhombic
Space group	Pnma	Pnma	Pnma	Pnma	Pnma	Pnma
Unit cell /Å	a = 10.349(3)	a = 10.349(3)	a = 10.5(1)	a = 10.329(8)	10.34(2)	10.48(4)
	b = 5.9940(2)	b = 5.9947(2)	b = 6.116(7)	b = 5.9899(5)	5.989(1)	6.124(2)
	c = 4.7066(1)	c = 4.7064(1)	c = 4.869(5)	c = 4.7022(4)	4.6995(9)	4.864(2)
Volume /$Å^3$	291.97(2)	291.99(2)	312.206	290.92(4)	291.13(9)	312.066
Density /$g \cdot cm^{-3}$	3.68	3.67	2.46	3.67	3.73	2.93
Strain (ε)	L* = 0.060(4)	L* = 0.055(3)	-	L* = 0.46(2) G* = 0.26(5)	L* = 1.11(5)	G* = 0.38(6)
R - factors	R_{wp} = 7.23 R_p = 5.72 R_{exp} = 55.64	R_{wp} = 6.90 R_p = 5.47 R_{exp} = 57.09		R_{wp} = 8.11 R_p = 6.23 R_{exp} = 64.41	R_{wp} = 9.63 R_p = 6.93 R_{exp} = 52.20	
GOF	0.13	0.12		0.13	0.18	

Percentages exclude the additional impurity phase
* L = Lorentzian; G = Gaussian

Table S3 The fractional coordinates, S.O.F. and B_{iso} of the $LiFePO_4$ phase for the 1sec sample.

Atom site	Atom type	Site symmetry	x	y	z	S.O.F.	B_{iso}
Fe1	Fe+2	4	0.28098	0.25	0.97442	0.99127	0.52017
P1	P	4	0.09492	0.25	0.41545	1	1.5
O1	O	4	0.09786	0.25	0.74253	1	0.71347
O2	O	4	0.44806	0.25	0.21121	1	0.50073
O3	O	8	0.16739	0.04026	0.2783	1	0.50122
Li1	Li	4	0	0	0	0.91139	1.48703
Fe2	Fe+3	4	0	0	0	0.08861	1.5

Table S4 The fractional coordinates, S.O.F. and B_{iso} of the $LiFePO_4$ phase for the 3sec sample.

Atom site	Atom type	Site symmetry	x	y	z	S.O.F.	B_{iso}
Fe1	Fe+2	4	0.28114	0.25	0.97448	0.99035	0.51253
P1	P	4	0.09424	0.25	0.41476	1	1.5
O1	O	4	0.09722	0.25	0.74255	1	0.6624
O2	O	4	0.44785	0.25	0.21201	1	0.59955
O3	O	8	0.16717	0.04047	0.27862	1	0.50122
Li1	Li	4	0	0	0	0.91183	1.48703
Fe2	Fe+3	4	0	0	0	0.08817	1.5

Table S5 The fractional coordinates, S.O.F. and B_{iso} of the $LiFePO_4$ phase for the 4sec sample.

Atom site	Atom type	Site symmetry	x	y	z	S.O.F.	B_{iso}
Fe1	Fe+2	4	0.27942	0.25	0.97185	0.96313	0.95644
P1	P	4	0.09343	0.25	0.41267	1	1.5
O1	O	4	0.10028	0.25	0.74696	1	1.34993
O2	O	4	0.44154	0.25	0.20807	1	0.50073
O3	O	8	0.16626	0.03318	0.27865	1	0.50122
Li1	Li	4	0	0	0	0.89893	0.61203
Fe2	Fe+3	4	0	0	0	0.10107	0.63631

Table S6 The fractional coordinates, S.O.F. and B_{iso} of the $LiFePO_4$ phase for the 5sec sample.

Atom site	Atom type	Site symmetry	x	y	z	S.O.F.	B_{iso}
Fe1	Fe+2	4	0.27791	0.25	0.9681	0.9534	0.71598
P1	P	4	0.08906	0.25	0.41294	1	1.5
O1	O	4	0.10384	0.25	0.75173	1	1.4375
O2	O	4	0.43413	0.25	0.21655	1	0.50073
O3	O	8	0.16792	0.02747	0.27849	1	0.50122
Li1	Li	4	0	0	0	0.83122	0.61203
Fe2	Fe+3	4	0	0	0	0.16878	0.5625

4. The bond valence sum to determine the oxidation state

The valence (ν) of Fe was calculated using the average bond distance (d) as follows:

$$v = e^{(R_0 - d)/B}$$

where R_0 and B are the bond valence parameters; B is considered as universal whereas R_0 depends on the atom identity. As recommended[1,2] the values of B = 0.37 Å and R_0 = 1.745 Å were used, where the latter was chosen based on the premise that the oxidation state of Fe is unknown. The values for d were obtained from Table 2 in the manuscript (i.e. the Fe-O interatomic distance). In an octahedral arrangement, the bond valence sum (BVS) is 6ν and the results are shown in Table S3.

Table S7 A summary of the bond valence sum for the different addition rate samples using the above-mentioned equation.

Sample	Valence	Bond valence sum
1sec	0.345	2.07
3sec	0.348	2.09
4sec	0.370	2.22
5sec	0.390	2.34

5. Mössbauer fits and χ^2 – values determined using Vinda

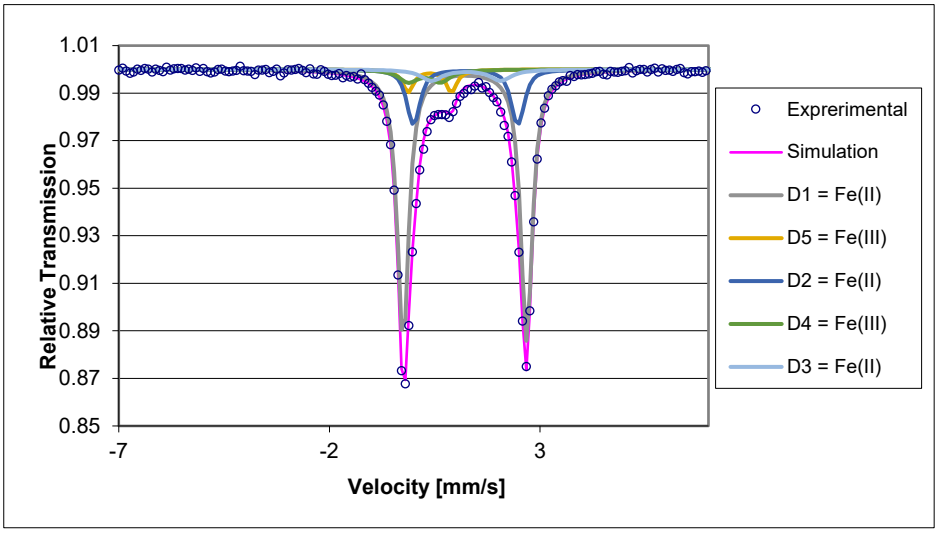

Fig. S7 Mössbauer spectrum of the 1sec sample as determined using Vinda.

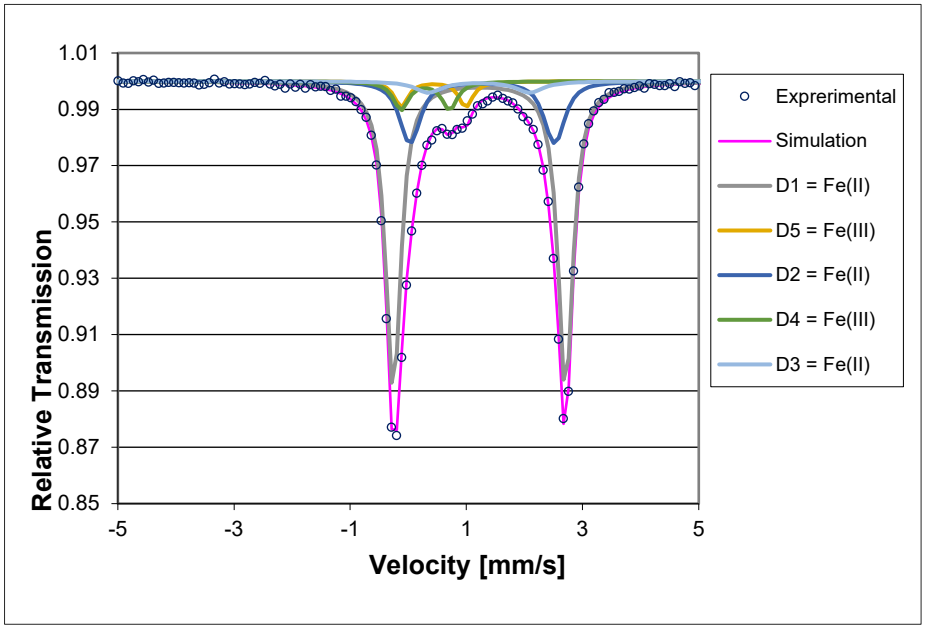

Fig. S8 Mössbauer spectrum of the 3sec sample as determined using Vinda.

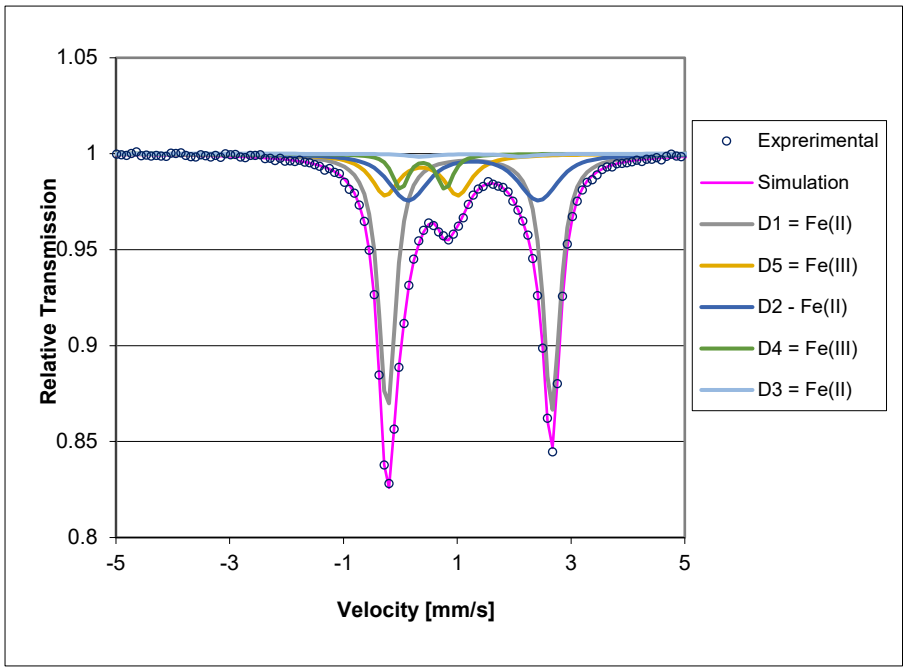

Fig. S9 Mössbauer spectrum of the 4sec sample as determined using Vinda.

Table S8 The χ^2 values indicating the goodness-of-fit for the Mössbauer spectra.

Sample	χ^2
1sec	1.43
3sec	1.36
4sec	1.04

6. EXAFS structural plots as determined using Artemis

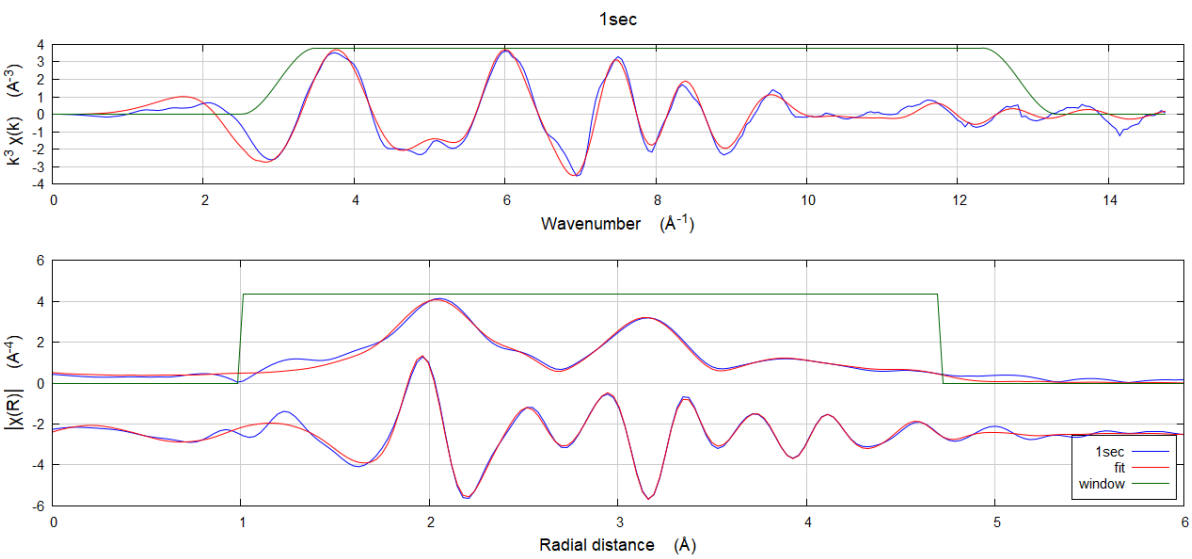

Fig. S10 The k-space, magnitude and real space of the Fourier Transform plots of the 1sec sample showing the experimental data, the fit and the range of the fitting window.

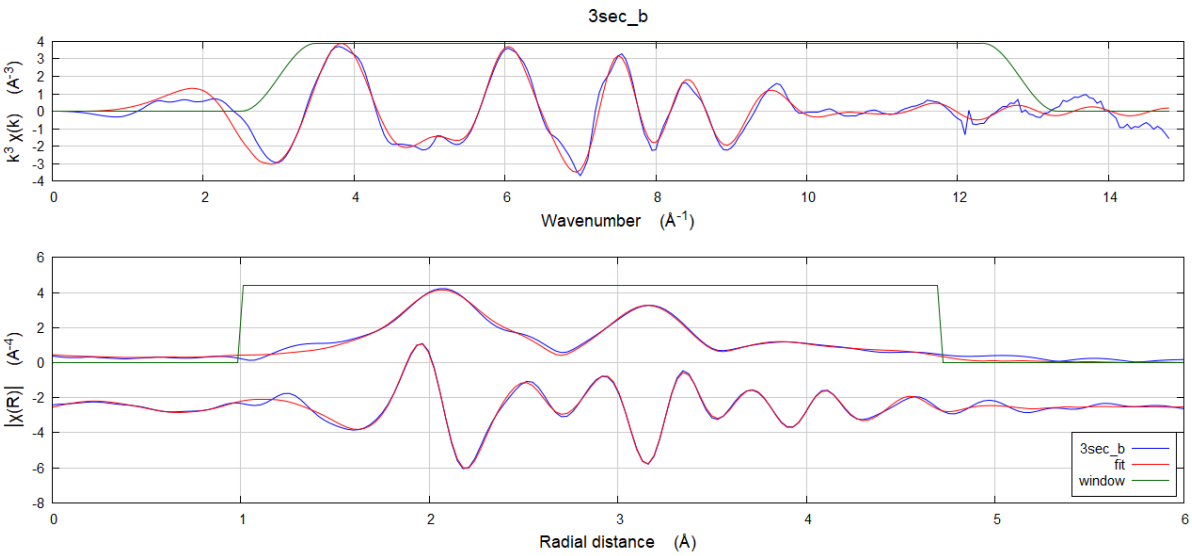

Fig. S11 The k-space, magnitude and real space of the Fourier Transform plots of the 3sec sample showing the experimental data, the fit and the range of the fitting window.

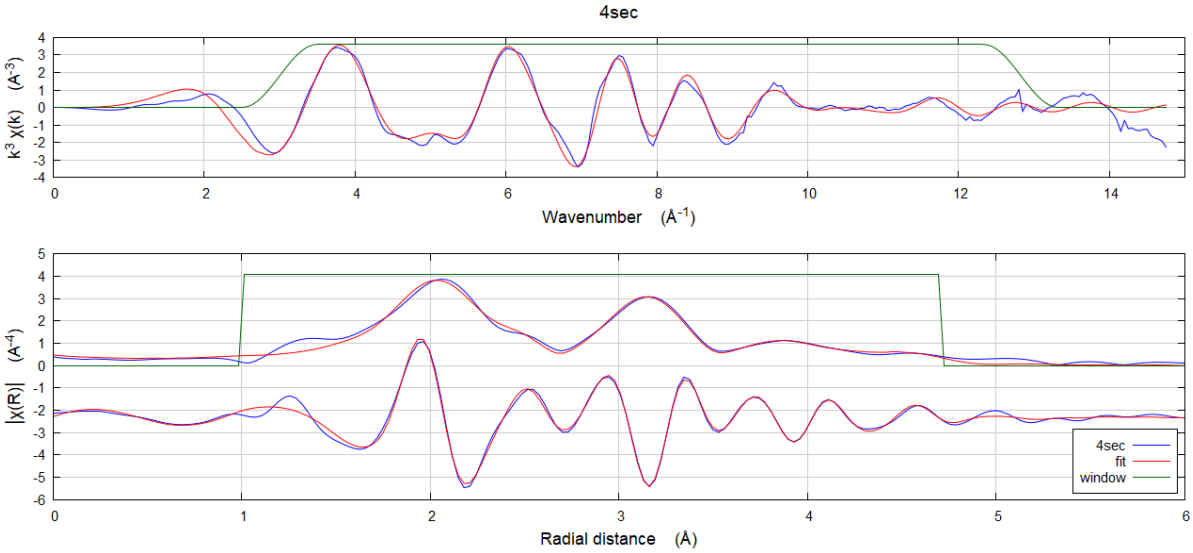

Fig. S12 The k-space, magnitude and real space of the Fourier Transform plots of the 4sec sample showing the experimental data, the fit and the range of the fitting window.

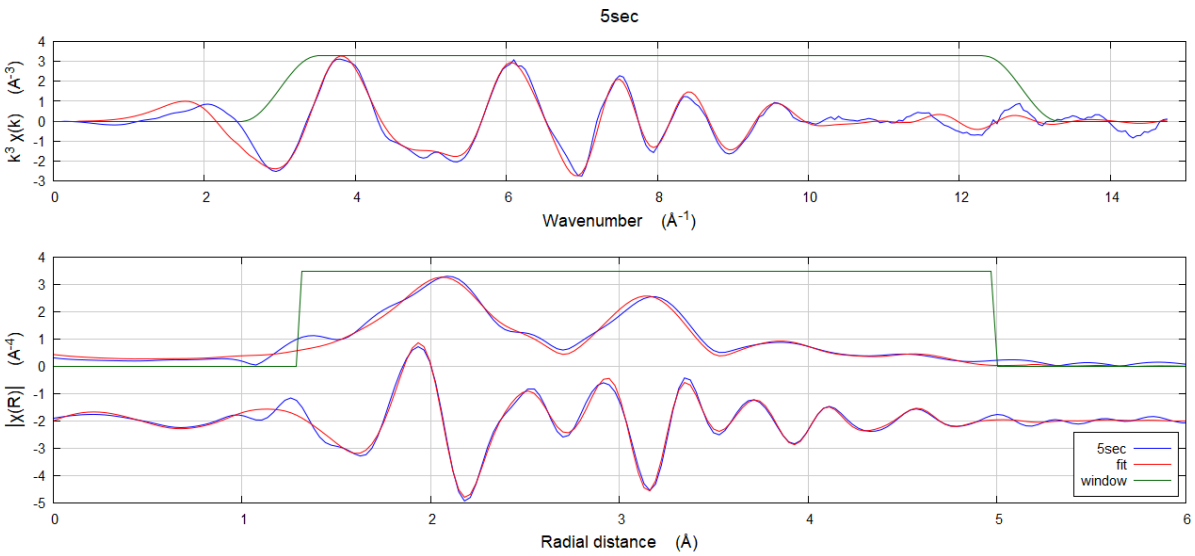

Fig. S13 The k-space, magnitude and real space of the Fourier Transform plots of the 5sec sample showing the experimental data, the fit and the range of the fitting window.

Table S9 Selected structural parameters extracted from the EXAFS fit of the different Li^+ addition rate samples.

	1sec	3sec	4sec	5sec
R-factor (%)	0.44	0.45	0.35	0.58
S_0^2	0.83(6)	0.90(9)	0.83(6)	0.76(2)
ΔE_0 (eV)	-0.8(8)	0.9(8)	-0.3(8)	-2.8(8)

In the EXAFS analyse 23 independent points were used to fit 14 parameters.

7. $LiFePO_4$ reference material

A commercially bought $LiFePO_4$ sample (Sigma Aldrich, >97%) was used as a reference material to compare the XANES region. In order to understand the characteristics of this material, the structure was also further analysed by other techniques where some were used in this study. An unidentified additional phase was detected in this material using PXRD (Fig. S13), Mössbauer spectroscopy (Fig. S14) and Raman spectroscopy (Fig. S16 and S17). The sextet environments found in the Mössbauer spectrum indicate that this additional phase could be Fe^{3+}-containing. Error indices extracted from a Rietveld refinement of the reference material can be found in Table S5. The lattice parameters and unit cell volume (Table S6) were comparable to those determined by other groups (Table S6), indicating that the impurity present does not have a large effect on the lattice parameters or volume. The higher R-factor for the EXAFS analysis can be due to the exclusion of this phase especially if this phase is Fe-containing (Fig. S15 and Table S8).

7.1. PXRD

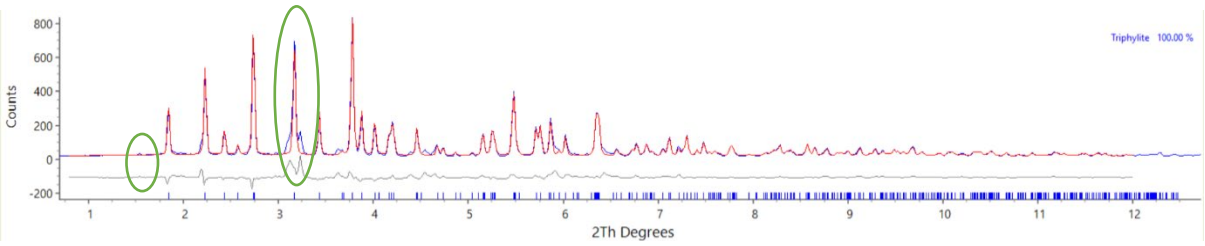

Fig. S14 Rietveld refinement plot of the reference $LiFePO_4$ sample. The impure phase/s is indicated with green on the diffractogram.

Table S10 Structural parameters extracted from a Rietveld refinement of the reference material.

R_{wp}	15.17
R_p	13.42
R_{exp}	9.20
GOF	1.13

Table S11 The lattice parameters and volume of $LiFePO_4$ reference material compared to other synthesised $LiFePO_4$ materials.

Reference	*a* /Å	*b* /Å	*c* /Å	Volume /Å^3
$LiFePO_4$ reference material	10.329(9)	6.0086(5)	4.6916(4)	291.19(4)
Prince *et al.*[3]	10.3095(7)	5.9993(4)	4.6932(3)	290.27(3)
Kuwahara *et al.*[4]	10.3280(5)	6.0040(3)	4.6936(2)	291.05(2)
Chen et al.[5]	10.334	6.004	4.694	291.24

7.2. Mössbauer spectroscopy

Three Voigt doublet (D1 – D3) environments were identified and two Lorentzian sextets (S1 – S2) were also added to improve the fit, but these did not account for all the smaller peaks on either side of the doublet. D1 was identified as Fe^{2+} in $LiFePO_4$,[6,7] D2 was also identified Fe^{2+} in $LiFePO_4$ but in a more distorted octahedra[8] and D3 was identified as Fe^{3+} on the M1 site.[8,9] The parameters for the sextets did not match those of α-Fe_2O_3[9] and Fe_3O_4.[10]

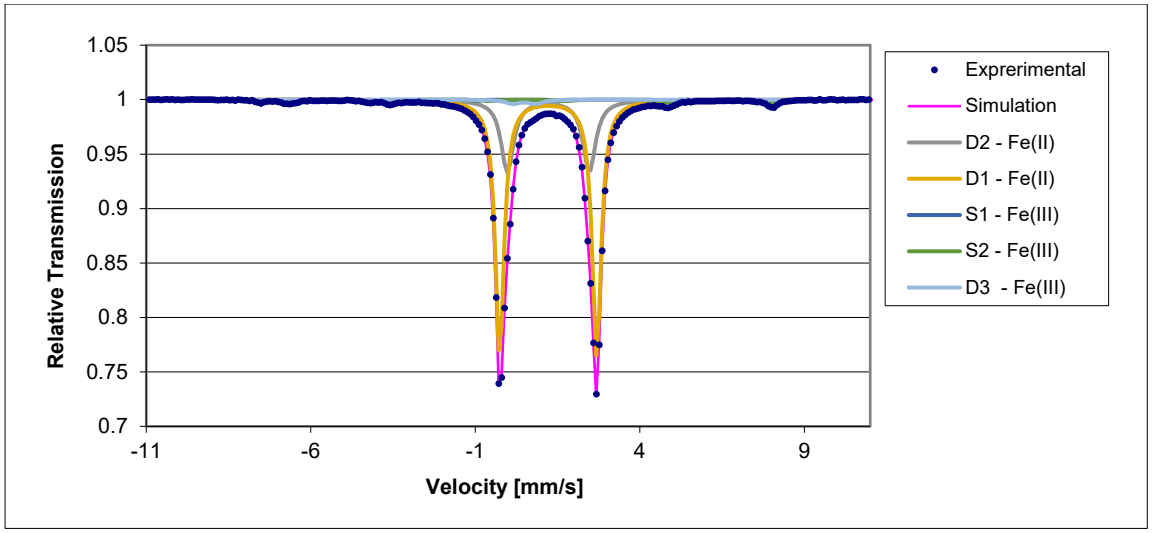

Fig. S15 Mössbauer spectrum of the $LiFePO_4$ reference material as determined using Vinda. D refers to the different doublets and S refers to the different sextet environments. $\chi^2 = 9.61$.

Table S12 Mössbauer parameters and area percentages of $LiFePO_4$ the reference material.

Fe environment	Isomer shift (δ – mm/s)	Quadrupole splitting (ΔE_Q – mm/s)	Percentage area (%)
D1 – Fe(II)	1.22(1)	2.95(1)	66(5)
D2 – Fe(II)	1.22(1)	2.49(1)	26(2)
D3 – Fe(II)	0.48(1)	0.69(1)	2(1)
S1 – Fe(III)	0.26(1)	-0.01(1)	2(1)
S1 – Fe(III)	0.62(1)	0.08(1)	4(1)

7.3. EXAFS

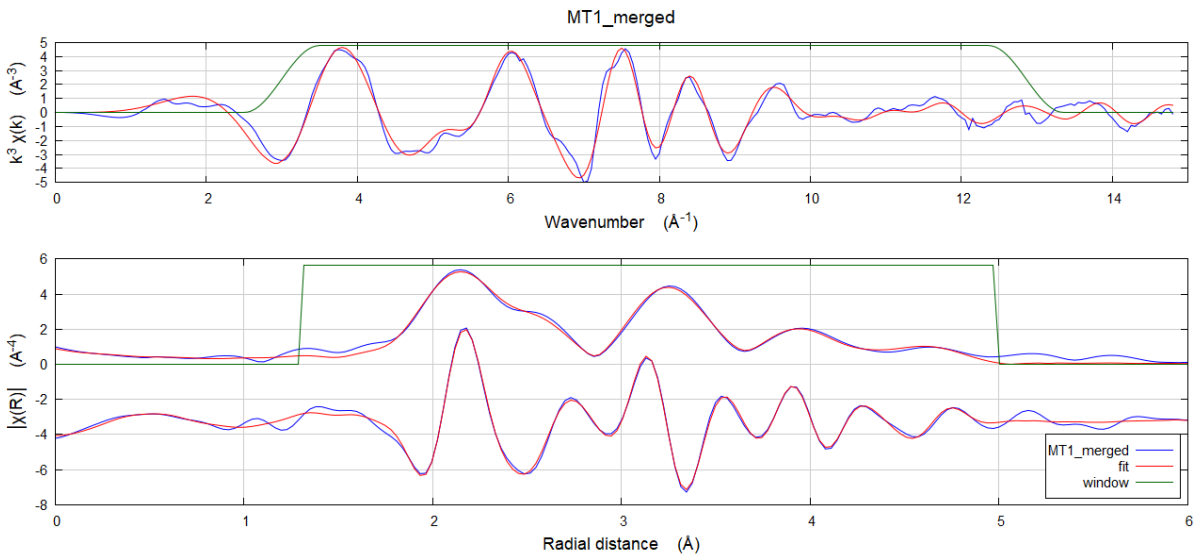

Fig. S16 The k-space, magnitude and real space of the Fourier Transform plots of the $LiFePO_4$ reference material showing the experimental data, the fit and the range of the fitting window.

Table S13 Selected structural parameters extracted from the EXAFS fit for the $LiFePO_4$ reference material.

	$LiFePO_4$ reference material
R-factor (%)	0.86
S_0^2	0.91(8)
ΔE_0 (eV)	0.22(10)

7.4. Raman spectroscopy

Two different coloured particulates were identified using Raman spectroscopy. The major phase was white (Fig. S16a) whereas the minor phase was black (Fig. S16b). The vibrational modes were identified for both phases. These modes were compared to the modes identified by Burba and Frech,[11] Paraguassu *et al.*[12] and Wu *et al.*[13] and the modes identified for the reference material is summarised in Table S9. $LiFePO_4$ was the major phase present in both coloured particulates. Three impurity phases were also detected, but one of those phases remained unidentified. Two modes can be associated with Fe_3O_4[14] although no other peaks were found for this impurity (shaded in green). Some modes can be associated with α-Fe_2O_3[14] (shaded in orange). These phases were included in the Mössbauer spectroscopy analysis. The hyperfine parameters for these phases did not improve the fit. The hyperfine parameters for the doublet identified as D3 also corresponds to the hyperfine parameters of superparamagnetic hematite.[15] This could possibly be the hematite detected in the samples.

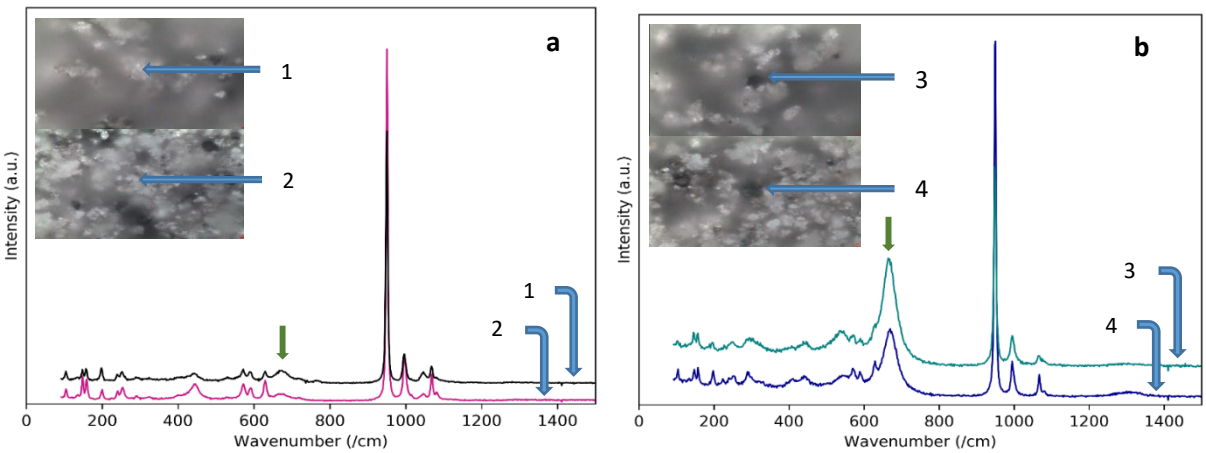

Fig. S17 Raman spectra for the $LiFePO_4$ reference material. Sampled areas consisted of (a) white particulates (labelled as 1 and 2) and (b) black particulates (labelled as 3 and 4). The green arrows indicate the intense peak that could be associated with Fe_3O_4.

Table S14 Raman modes for the white and black particulates present in the $LiFePO_4$ reference material. $LiFePO_4$ modes are shaded in blue, α-Fe_2O_3 in orange, Fe_3O_4 in green and the unidentified phases are not shaded.

Wavenumbers(/cm)				Assignment
LFP (1)	LFP (2)	LFP (3)	LFP (4)	
104	104	103	102	PO_4^{3-} rotational and Fe^{2+} translational motion
134*		134*		
148	147	147	146	
158	157	157	156	
199	197	197	195	
		223	227	
240	239			
253	251	254	247	
290	289	291	299	
		408		υ_2 (PO_4^{3-})
444	443	441	442	
	530	549		
571	571	571	571	υ_4 (PO_4^{3-})
591	589	590	591	
629	629	628	626	
672	672	669	667	
719*	720*			
949	950	948	947	υ_1 (PO_4^{3-})
998	998	995	995	υ_3 (PO_4^{3-})
1045*	1045*			
1068	1067	1066	1067	
1082*		1080*		
		1306	1307	

8. References

1. S. M. Kanowitz and G.J. Palenik, *Inorg. Chem.,* 1998, **37**, 2086–2088.
2. S. Z. Hu and Z. H. Zhou, *Zeitschrift fur Krist.,* 2004, **219**, 614–620.
3. A. A. M. Prince, S. Mylswamy, T. S. Chan, R. S. Liu, B. Hannoyer, M. Jean, C.H. Shen, S. M. Huang, J. F. Lee and G. X. Wang, *Solid State Commun.*, 2004, **132**, 455–458.
4. A. Kuwahara, S. Suzuki and M. Miyayama. *J. Electroceramics*, 2010, **24**, 69–75.
5. J. Chen, S. Wang and M. S. Whittingham, *J. Power Sources,* 2007, **174**, 442–448.
6. M. Maccario, L. Croguennec, A. Wattiaux, E. Suard, F. Le Cras and C. Delmas, *Solid State Ionics*, 2008, **179**, 2020–2026.
7. A. Yamada, S. C. Chung and K. Hinokuma. *J. Electrochem. Soc.*, 2001, **148**, A224.
8. R. Amisse, M. Sougrati, L. Stievano, C. Davoisne, G. Dražič, B. Budič, R. Dominko and C. Masquelier, *Chem. Mater.*, 2015, **27**, 4261–4273.
9. S. Hamelet, P. Gibot, M. Casas-Cabanas, D. Bonnin, C. P. Grey, J. Cabana, J. B. Leriche, J. Rodriguez-Carvajal, M Courty, S. Levasseur, P. Carlach, M. Van Thournout, J. M.

Tarascon and C. Masquelier, *J. Mater. Chem.*, 2009, **19**, 3979–3991.
10. J. Winsett, A. Moilanen, K. Paudel, S. Kamali, K Ding, W. Cribb, D. Seifu, S. Neupane. *SN Appl. Sci.*, 2019, **1**, 1–8.
11. C. M. Burba and R. Frech. Raman and FTIR Spectroscopic Study of Li_xFePO_4 ($0 \leq x \leq 1$). *J. Electrochem. Soc.*, 2004, **151**, A1032.12. W. Paraguassu, P. T. C. Freire, V. Lemos, S. M. Lala, L. A. Montoro and J. M. Rosolen. *J. Raman Spectrosc.*, 2005, **36**, 213–220.
13. J. Wu, G. Krishna Phani Dathar, C. Sun, M. G. Theivanayagam, D. Applestone, A. G. Dylla, A. Manthiram, G. Henkelman, J. B. Goodenough, J. B. and K. J. Stevenson. K. J. *IOP Publ. Nanotechnol. Nanotechnol.*, 2013, **24**, 424009–424018.
14. D. L. A. de Faria and F. N. Lopes. *Vib. Spectrosc.,* 2007*,* **45**, 117–121.
15. L. C. Sánchez, J. D. Arboleda, C. Saragovi, R. D. Zysler and C. A. Barrero. *Phys. B Condens. Matter*, 2007, **389**, 145–149.